Anisotropic Diffusion in Mitral Cell Dendrites Revealed by Fluorescence Correlation Spectroscopy

Arne Gennerich and Detlev Schild
Physiologisches Institut, Universität Göttingen, D 37073 Göttingen, Germany.

ABSTRACT Fluorescence correlation spectroscopy (FCS) can be used to measure kinetic properties of single molecules in drops of solution or in cells. Here we report on FCS measurements of tetramethylrhodamine (TMR)-dextran (10 kDa) in dendrites of cultured mitral cells of *Xenopus laevis* tadpoles. To interpret such measurements correctly, the plasma membrane as a boundary of diffusion has to be taken into account. We show that the fluorescence data recorded from dendrites are best described by a model of anisotropic diffusion. As compared to diffusion in water, diffusion of the 10-kDa TMR-dextran along the dendrite is slowed down by a factor 1.1–2.1, whereas diffusion in lateral direction is 10–100 times slower. The dense intradendritic network of microtubules oriented parallel to the dendrite is discussed as a possible basis for the observed anisotropy. In somata, diffusion was found to be isotropic in three dimensions and 1.2–2.6 times slower than in water.

INTRODUCTION

Fluorescence correlation spectroscopy (FCS) can be used to study kinetic properties of single molecules (Schwille et al., 1997; Widengren and Rigler, 1998; Schwille, 2001). If such measurements are done in cells or cell processes, the volume from which fluorescence is gathered is important because it can be on the same order of magnitude or smaller than the volume of the excitation laser focus. In such systems, the confinement of diffusion by the plasma membrane has to be taken into account (Gennerich and Schild, 2000).

We investigate diffusion of single molecules in dendrites after loading cultured neurons with tetramethylrhodamine (TMR)-dextran through a patch pipette. Surprisingly, autocorrelation analysis of dendritic fluorescence clearly suggested the presence of more than one molecular species, although only one species was loaded into the cytosol.

We solve this apparent contradiction by extending the FCS model of confined diffusion to the case of anisotropic diffusion. Fitting dendritic FCS data to this diffusion model indicated the presence of just one molecular species. Anisotropic diffusion in dendrites could be expected because the known intradendritic microtubular network might hamper diffusion orthogonally to the microtubules while leaving it largely unaffected in the longitudinal direction.

MATERIALS AND METHODS

Cell culture

Cultured neurons of the olfactory bulb (OB) of *Xenopus laevis* were prepared as described previously by Bischofberger and Schild (1995). Briefly, larvae of *Xenopus laevis* (stage 48–54, Nieuwkoop and Faber, 1956) were anesthetized with Tricain (100 mg/l), and the OBs were extirpated. The tissue was incubated at 22°C for 90 min in a dissociation solution containing EDTA (1 mM), papain (30 U/ml), and cysteine (1.5 mM). The resulting pieces were triturated with an Eppendorf pipette. The cells were plated onto dishes coated with poly-L-lysine (50 μg/ml) and laminin (20 μg/ml) in a drop of medium (50 μl, L15 (Leibovitz), Life Technologies, Karlsruhe, Germany) containing 70% L15, 10% horse serum, and 50 μg/ml gentamycin. After 20 h, 0.1 ml growth medium, which contained 75% L15, 5% horse serum, and 50 μg/ml gentamycin, was added, allowing the cells to condition their environment. Measurements were carried out within 2 weeks after plating.

The cultured cells were characterized by the use of antibodies against glial cells and GABAergic neurons. Mitral cells were identified by injection of fluorescent beads into the lateral olfactory tract and subsequent retrograde labeling (Bischofberger et al., 1995). The results were very similar to those reported for rat-cultured OB cells (Trombley and Westbrook, 1990); mitral cells appeared as the largest neurons in the culture and were multipolar, whereas glutamic acid decarboxylase-positive cells were smaller and of ellipsoidal shape. Both cell types had large nuclei filling most of the soma. All FCS measurements taken in the soma were thus performed in the nucleus.

Electrophysiology

Standard patch clamp equipment was used as described (Czesnik et al., 2001). To load the neurons with the fluorescent dye TMR-dextran (10 kDa, Molecular Probes, Leiden, the Netherlands), the neurones were patch clamped in the whole cell configuration using borosilicate glass pipettes having pipette resistances of ~6 MΩ. To check for the stationarity of the experimental conditions we measured the holding current and cell resistance over the entire duration of an FCS recording. The compostition of the bath solution was (in mM): NaCl 102, KCl 2, $MgCl_2$ 2, $CaCl_2$ 2, Glucose 20, HEPES 10, 240 mOsm, pH 7.8, whereas that of the pipette solution was NaCl 2, KCl 103, $MgCl_2$ 3, EGTA 1, HEPES 10, K_2-ATP 1, Na_2-GTP 0.01, 220 mOsm, pH 7.8.

Transmission electron microscopy

For transmission electron microscopy, the tadpoles were perfused with 1.5% glutaraldehyde (Sigma-Aldrich Chemie, Deisenhofen, Germany) in 0.05 M cacodylic buffer (pH 7.4) through the tail vein for 15 min. Brains were removed and stored in the same fixative for several days at 10°C. Forebrains were dissected, postfixed in 2% osmium tetroxide in the same

Submitted November 20, 2001 and accepted for publication March 13, 2002.

Address reprint requests to Detlev Schild, Physiologisches Institut, Universität Göttingen, Humboldtallee 23, D 37073 Göttingen, Germany. Tel: +49-551-395915; Fax: +49-551-398399; E-mail: dschild@gwdg.de.

0006-3495/02/07/510/13 $2.00

buffer for 2 h at room temperature, dehydrated through alcohol and propylene oxide, and embedded into Poly/Bed 812 Embedding Media (Polysciences, Warrington, PA). Ultrathin sections were cut with diamond knives on a SORVALL MT2-B Ultra-Microtome (DuPont, Wilmington, DE), collected on copper slot grids provided with formvar support films, counterstained with uranilacetate and lead citrate and examined in JEM100-CX transmission electron microscope (JEOL, Tokyo, Japan). Negatives were scanned using a flatbed scanner at 600 DPI (SNAPSCAN 1236, AGFA, Köln, Germany), and imported into Adobe Photoshop 6.0 for layout.

FCS set-up

The FCS apparatus was attached to a modified inverted Zeiss Axiovert 35 microscope (Carl Zeiss, Göttingen, Germany) with a C-Apochromat 40/1.2 W (Carl Zeiss). A HeNe cw-laser (2.2 mW) at 543.5 nm was used as excitation source (LK 54015, Laser Graphics, Dieburg, Germany). The back aperture was not overilluminated. The laser intensity in the focal plane was set to 3.14 kW/cm^2. This power affected neither the appearance of the neuron under investigation nor its electrophysiological properties. Tandem galvanometer mirrors (GD120DT, GSI Lumonics, Unterschleissheim, Germany) were used for *x–y* positioning, and a piezo-driven objective holder (P-721.10, Physik Instrumente, Waldbronn, Germany) was used for *z* positioning. The voltages to the *xy* scanner and the *z* piezo were controlled either by potentiometers or by a custom program written in C and running on a Siemens microcontroller (MCB-167, Keil Elektronik, Grasbrunn, Germany), to which a 12-bit dual-channel DAC (DAC 2813AP, Burr & Brown, Tucson, AZ) was latched. The detection pinhole had a diameter of 50 μm. The beamwaist radius and the structure factor were determined to be $r_{xy} = 0.24$ μm and $S = r_z/r_{xy} = 7$ by measuring the translational three-dimensional (3D)-diffusion of TMR (T-5646, Sigma-Aldrich Chemie) in water, assuming a diffusion constant of $D = 2.8 \times 10^{-6}$ cm^2/s (Rigler et al., 1993). The dark count rate of the avalanche photodiode used (SPCM-AQ-141, EG&G, Optoelectronics, Dumberry, Canada) was 100 s^{-1}, its photon-detection efficiency was 70–80%. Back-reflexion ($\lambda_{exc} = 543.5$ nm) was blocked by an interference filter (HQ 582/50, OD6, AF Analysetechnik, Pfrondorf, Germany) put in front of the photodiode. The output pulses of the photon-counting module were fed to a correlator board (ALV-5000/E, ALV, Langen, Germany).

Data analysis

Autocorrelation functions (ACFs) were calculated by the correlator board and saved as ASCII files. The ACFs were analyzed either with Origin (Microcal Software, Northhampton, MA) in case of analytical fitting functions or with Mathematica (Mathematica 4.0, Wolfram Research, Champaign, IL) in case of nonanalytical functions (e.g., Eq. 6).

Size of dendrites

The geometry of dendrites was determined in two different ways. First, the dendritic diameter was entered as a free parameter into the model of confined diffusion and thus resulted from the fit (see below, Theory). Second, a line-scan profile across a dendrite was taken as an independent measure of dendritic size.

After an FCS measurement, the cultured neurons were incubated for ~3 min in 20 μM di-8-ANNEPS (Molecular Probes) dissolved in the bath solution. After flushing the bath, we scanned along a line orthogonal to the dendrite. An example of the resulting intensity profile is shown in Fig 1 *A*. This curve was best described by a *y*-line scan profile for a rectangular dendritic cross section $s_{rect}(y)$ as given by Gennerich and Schild (2000),

$$s_{rect}(y) = \alpha\Bigg[\exp\left(-\frac{d_z^2}{2r_z^2}\right)\left\{\mathrm{erf}\left(\sqrt{2}\,\frac{y - y_0 + d_y/2}{r_{xy}}\right) - \mathrm{erf}\left(\sqrt{2}\,\frac{y - y_0 - d_y/2}{r_{xy}}\right)\right\} + S \times \mathrm{erf}\left(\frac{d_z}{\sqrt{2}r_z}\right)\left\{\exp\left(-2\,\frac{(y - y_0 + d_y/2)^2}{r_{xy}^2}\right) + \exp\left(-2\,\frac{(y - y_0 - d_y/2)^2}{r_{xy}^2}\right)\right\}\Bigg], \quad (1)$$

where

$$\alpha = gQI_0\langle C_s\rangle\,\frac{\pi}{2}\,r_{xy}^2, \quad (2)$$

with $\langle C_s\rangle$ being the average number of dye molecules per surface element. g accounts for the overall optical losses of the emission pathway, including the efficiency of the photoavalanche diode, and Q is the quantum efficiency of the fluorescent dye. I_0 is the maximum laser intensity in the focus. $y = y_0$ and $z = 0$ are the center of the dendritic cross section with width d_y and height d_z. Assuming a circular dendritic cross section $s_{circ}(y)$ (Gennerich and Schild, 2000) gave a much worse fit to the data (Fig. 1 *A*), presumably because the adhesion between dendrite and Petri dish leads to an approximately rectangular shape at the base of the dendrite.

Occasionally, there were dendrites that were best modeled by a circular dendritic cross section (Fig. 1 *B*). For a dendrite homogeneously filled with a fluorescent dye, the theoretical profile follows from the convolution product,

$$s'(y) = \langle C\rangle\int_{-\infty}^{+\infty} dx' \int_0^{+\infty} dr \int_0^{2\pi} d\varphi\; r\;\xi_{circ}(r) \times I_E(x', y - r\cos\varphi, r\sin\varphi), \quad (3)$$

of the excitation volume, given by the detectable emission intensity distribution $I_E(x, y, z)$ (Rigler et al., 1993),

$$I_E(x, y, z) = gQI_0\exp\left(-2\,\frac{x^2 + y^2}{r_{xy}^2}\right)\exp\left(-2\,\frac{z^2}{r_z^2}\right), \quad (4)$$

and a circular boundary function in the *y–z* plane orthogonal to the dendrite,

$$\xi_{circ}(r) = \Theta(R - r) = \begin{cases} 1 & \text{for} \quad r \le R \\ 0 & \text{otherwise,} \end{cases} \quad (5)$$

whereby we have used cylinder coordinates, x', $y' = r\cos\varphi$ and $z' = r\sin\varphi$. For the circular cross section, we thus have

$$s'_{circ}(y) = \vartheta\exp[-2(y - y_0)^2/r_{xy}^2]\int_0^R dr\int_0^{2\pi} d\varphi\; r \times \exp[-2\{r^2\cos^2\varphi - 2(y - y_0)r\cos\varphi + r^2\sin^2\varphi/S^2\}/r_{xy}^2], \quad (6)$$

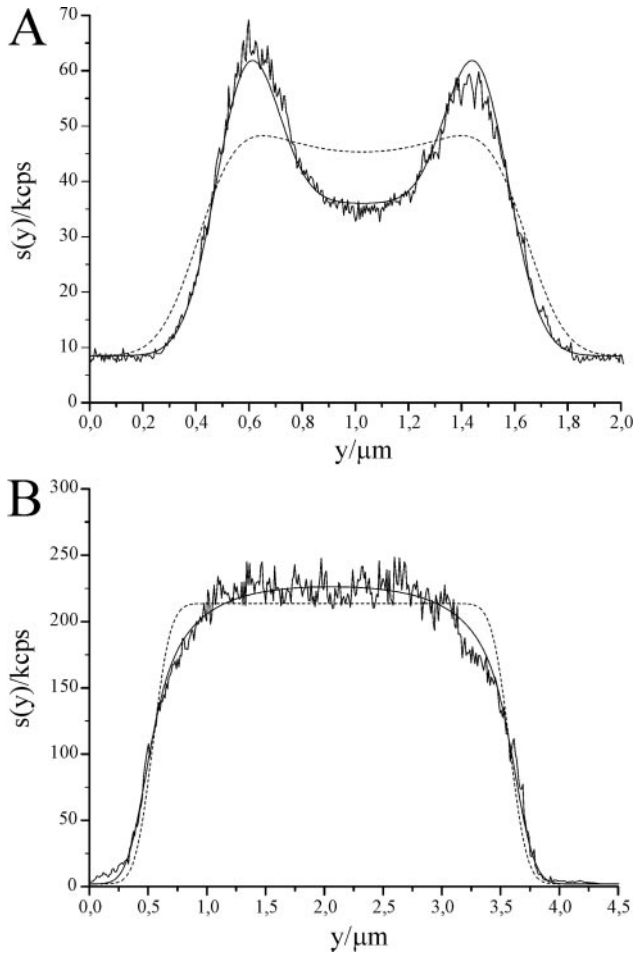

FIGURE 1 Line-scan profiles taken from dendrites of cultured mitral cells. (*A*) Line-scan through a dendrite stained with di-8-ANNEPS (*noisy trace*); scan velocity: 32 nm/s. The solid curve shows the fitted theoretical line-scan profile $s_{rect}(y)$ (Eq. 1) for a rectangular dendritic cross section. Result of the fit: $\alpha = 15.31$ kcps, $d_y = 0.895$ μm, $d_z = 0.761$ μm, $y_0 = 1.026$ μm, and $I_B = 8.464$ kcps, respectively (fixed parameters: $r_{xy} = 0.236$ μm and $r_z = 1.652$ μm). Fitting the theoretical line-scan profile $s_{circ}(y)$ for a circular cross section (*dashed*) gave $\alpha = 23.97$ kcps and $d = 1.22$ μm, respectively (fixed parameters: $r_{xy} = 0.236$ μm, $r_z = 1.652$ μm, $y_0 = 1.026$ μm, and $I_B = 8.464$ kcps). (*B*) Line-scan through a thick dendrite that was homogeneously filled with 10 kDa TMR-dextran (*noisy trace*); scan velocity: 38 nm/s. The theoretical line-scan profile $s'_{circ}(y)$ (Eq. 6) for a circular dendritic cross section was fitted (*solid curve*) to the experimental line-scan profile. Result of the fit: $\vartheta = 384.71$ kcps/μm^2, $R = 1.636$ μm, and $y_0 = 2.053$ μm, respectively. Fitting the theoretical line-scan profile $s'_{rect}(y)$ (Eq. 8) for a rectangular cross section (*dashed curve*) gave $\beta = 105.5$ kcps, $d_y = 3.035$ μm, and $y_0 = 2.058$ μm (fixed parameters: $r_{xy} = 0.236$ μm, $S = 7$, and $I_B = 2.2$ kcps).

where

$$\vartheta = \langle C\rangle g Q I_0 \pi^{1/2} r_{xy}, \tag{7}$$

and $y = y_0$ and $z = 0$ give the center of the dendritic cross section. Fitting this function to the profile shown in Fig. 1 *B* shows that this profile is well described by a circular cross section. In this case, the alternative fit for a rectangular dendritic cross section, (Gennerich and Schild, 2000),

$$s'_{rect}(y) = \beta\left[\mathrm{erf}\left(\sqrt{2}\,\frac{y - y_0 + d_y/2}{r_{xy}}\right) - \mathrm{erf}\left(\sqrt{2}\,\frac{y - y_0 - d_y/2}{r_{xy}}\right)\right] \tag{8}$$

with

$$\beta = g Q I_0 \langle C\rangle r_{xy}^2 r_z \frac{\pi^{3/2}}{2^{5/2}}\,\mathrm{erf}\left(\frac{d_z}{\sqrt{2}r_z}\right), \tag{9}$$

was unsatisfactory. This was presumably due to the low adhesion of the dendritic plasma membrane to the Petri dish.

THEORY

Standard FCS model

The ACF for Brownian diffusion of m noninteracting fluorescent species in the case of an open Gaussian-shaped detection volume V_d, $V_d = \pi^{3/2} r_{xy}^2 r_z$, is given by (Aragón and Pecora, 1976; Rigler et al., 1993)

$$G(\tau) = G_{xyz}(\tau) := \frac{1}{\langle N_{tot}\rangle}\left(1 + \frac{T e^{-\tau/\tau_T}}{1 - T}\right) \times \sum_{j=1}^{m} \frac{\Phi_j}{1 + \tau/\tau_{diff_j}} \times \frac{1}{\sqrt{1 + \tau/S^2\tau_{diff_j}}}, \tag{10}$$

where T and τ_T account for the fractional part of molecules being in the triplet state and the triplet-state decay time constant, respectively (Widengren et al., 1995). Φ_j, is the fractional weighting factor (Elson and Magde, 1974) and $\tau_{diff_j} := r_{xy}^2/4D_j$ the characteristic diffusion time constant for the jth species with diffusion constant D_j, respectively.

FCS model for confined diffusion

In the case of a diffusion space with a width or height on the same order of magnitude or smaller than the detection volume V_d, the confinement of diffusion has to be taken into account. In case of a sufficiently small dendritic height d_z, i.e., $d_z/r_z \leq 0.833$ (Gennerich and Schild, 2000), the diffusion in z direction (optical axis) can be neglected. In case of FCS measurements made in dendrites with diameters of 1 μm or less, diffusion in the axial direction was neglected, because, with $r_{xy} \cong 0.24$ μm and $S = 7$, i.e., $r_z = 1.7$ μm, d_z/r_z was smaller than 0.59.

Under these conditions, the ACF model for diffusion in small dendrites for m noninteracting fluorescent species becomes

$$G(\tau) = \frac{1}{\langle N_{tot}\rangle}\left(1 + \frac{T e^{-\tau/\tau_T}}{1 - T}\right) \times \sum_{j=1}^{m} \Phi_j \times g_x^j(\tau) \times \bar{g}_{y*}^j(\tau), \tag{11}$$

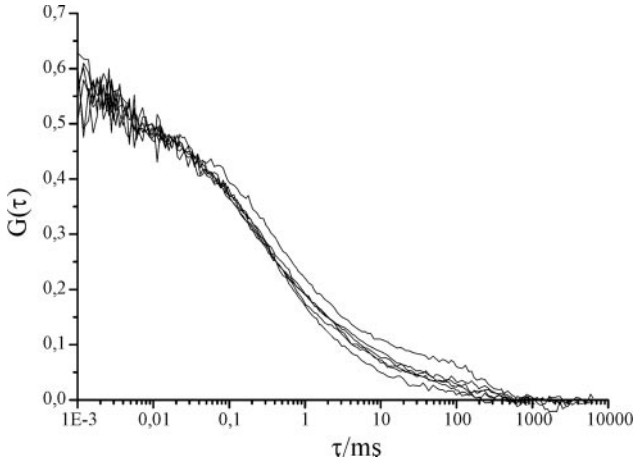

FIGURE 2 Autocorrelation plots of fluorescence fluctuations of 10 kDa TMR-dextran emitted from a dendrite of a cultured neuron of the OB (the line-scan profile of this dendrite is shown in 1 *A*). The duration of each FCS measurement was 10 s. The time delay between two measurements was ~10 s. The measurements were carried out in the same dendritic compartment after diffusion had reached a steady state.

with m standard ACF terms for diffusion along the dendrite, i.e., the x axis,

$$g_x^j(\tau) := (1 + \tau/\tau_{diff_j})^{-1/2}, \tag{12}$$

and m ACF terms $\bar{g}_{y^*}^j(\tau)$ for confined diffusion along the y axis,

$$\bar{g}_{y^*}^j(\tau) = \frac{\sqrt{\pi}}{Y}\left[1 + \left(\frac{Y}{\sqrt{\pi}} \times \frac{\mathrm{erf}(Y)}{\mathrm{erf}^2(Y/\sqrt{2})} - 1\right) \times \frac{\exp[-k(Y)(\pi/Y)^2\tau/\tau_{diff_j}]}{\sqrt{1 + \tau/\tau_{diff_j}}}\right], \tag{13}$$

with

$$k(Y) = 0.689 + 0.34\exp[-0.37(Y - 0.5)^2]. \tag{14}$$

The confinement parameter Y is given by the ratio of the width d_y of the dendrite to the radius r_{xy} of the open detection volume in the focal plane, i.e., $Y := d_y/r_{xy}$ (for more details, and for an expression of $\bar{g}_{y^*}^j(\tau)$, Eq. 13, that does not require the calculation of error functions, see Gennerich and Schild, 2000).

FCS models for anisotropic diffusion

In anisotropic media, the diffusion along and perpendicular to the x axis is characterized by different diffusion constants $D_x = D_\parallel$ and $D_y = D_z = D_\perp$, and the ACF model for unconfined diffusion of one species becomes

$$G(\tau) = \frac{1}{\langle N\rangle}\left(1 + \frac{Te^{-\tau/\tau_T}}{1 - T}\right) \times \frac{1}{\sqrt{1 + \tau/\tau_{diff_\parallel}}} \times \frac{1}{\sqrt{1 + \tau/\tau_{diff_\perp}}} \times \frac{1}{\sqrt{1 + \tau/S^2\tau_{diff_\perp}}}, \tag{15}$$

with $\tau_{diff_\parallel} := r_{xy}^2/4D_\parallel$ and $\tau_{diff\perp} := r_{xy}^2/4D_\perp$. For diffusion detectable only along the x axis, this model reduces to

$$G_x(\tau) = \frac{1}{\langle N\rangle}\left(1 + \frac{Te^{-\tau/\tau_T}}{1 - T}\right) \times \frac{1}{\sqrt{1 + \tau/\tau_{diff_\parallel}}}. \tag{16}$$

The model for confined diffusion of one fluorescent species (Eq. 11, $m = 1$)

$$G(\tau) = \frac{1}{\langle N\rangle}\left(1 + \frac{Te^{-\tau/\tau_T}}{1 - T}\right) g_x(\tau)\bar{g}_{y^*}(\tau) \tag{17}$$

can easily be extended to a model for anisotropic diffusion by replacing Eqs. 12 and 13 by

$$g_x(\tau) := (1 + \tau/\tau_{diff_\parallel})^{-1/2} \tag{18}$$

and

$$\bar{g}_{y^*}(\tau) = \frac{\sqrt{\pi}}{Y}\left[1 + \left(\frac{Y}{\sqrt{\pi}} \times \frac{\mathrm{erf}(Y)}{\mathrm{erf}^2(Y/\sqrt{2})} - 1\right) \times \frac{\exp[-k(Y)(\pi/Y)^2\,\tau/\tau_{diff_\perp}]}{\sqrt{1 + \tau/\tau_{diff_\perp}}}\right]. \tag{19}$$

FCS model for single transition events

The linear transition of a single molecule, e.g., a large autofluorescent species, through the detection volume is a deterministic process. It can cause a detectable intensity spike and, therefore, lead to a transient ACF contribution. The intensity change $\delta i(t)$ upon a linear translation of a fluorescent particle through the focus volume is given by the convolution product of the excitation volume $I_E(x, y, z)$ (Eq. 4) and the boundary function of the fluorescent particle. If a small particle (diameter $d \ll r_{xy}$) travels along the x axis, the intensity change is given by

$$\delta i(t) \sim \exp\left(-2\frac{v^2t^2}{r_{xy}^2}\right), \tag{20}$$

if the particle crosses the center of the detection volume at $t = 0$ and v is the particle velocity.

In this case, the ACF contains a transient component proportional to

$$g_{STE}(\tau) = e^{-(\tau/\tau_t)^2}, \tag{21}$$

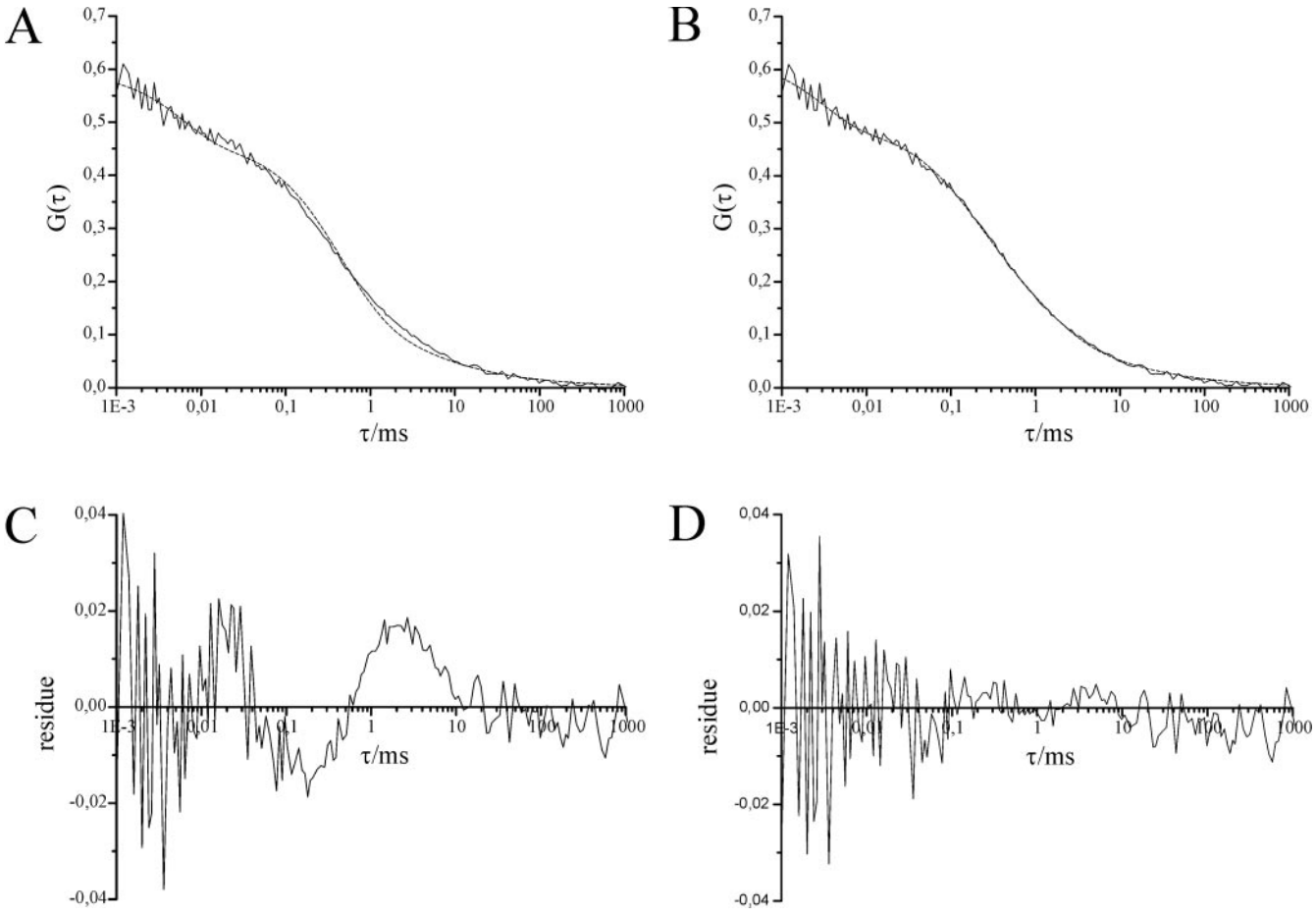

FIGURE 3 Autocorrelation function calculated from fluorescence fluctuations of 10 kDa TMR-dextran emitted from a dentrite of a cultured neuron of the OB (identical to the lowest trace shown in Fig. 2). (*A*) Fitting a one-component model for confined diffusion (Eq. 11, $m = 1$, *dashed curve*) gave $\langle N \rangle = 2.164$, $T = 0.223$, $\tau_T = 6.05$ μs, and $\tau_{diff_1} = 0.515$ ms (fixed parameter: $Y = d_y/r_{xy} = 3.79$, taken from the line-scan measurement of this dendrite, Fig. 1 *A*). (*B*) Fitting a two-component model (Eq. 11, $m = 2$, *dashed curve*) gave $\langle N_{tot} \rangle = 2.028$, $T = 0.208$, $\tau_T = 3.01$ μs, $\Phi_1 = 0.598$, $\tau_{diff_1} = 0.185$ ms, and $\tau_{diff_2} = 1.422$ ms (fixed parameter: $Y = 3.79$). (*C*) Residuals of the least square fit shown in *A*. (*D*) Residuals of the fit shown in *B*. The dendritic dye concentration was calculated to be 25 nM ($\langle C \rangle = \langle N_{tot} \rangle / V_d^* N_A$, $N_A = 6.02 \times 10^{23}$/Mol, and $V_d^* = 0.133$ fl obtained from $V_d^* = \pi^{3/2} r_{xy} r_z [\mathrm{erf}(Y/\sqrt{2})]^2 / \mathrm{erf}(Y) \times [\mathrm{erf}(Z/\sqrt{2})]^2/\mathrm{erf}(Z)$, and $Z = d_z/r_z = 0.461$, see Gennerich and Schild, 2000).

where the characteristic "transition" time τ_t is defined by $\tau_t := r_{xy}/v$. Due to the averaging over time, this component fades with time. The same expression was obtained by Magde et al. (1978) for the stationary stochastic process of uniform translations of fluorescent particles.

RESULTS

Time constants of dendritic diffusion

We measured the ACF of fluorescence fluctuations of 10 kDa TMR-dextran in dendrites of cultured neurons of the OB. The ACFs of subsequent measurements in the same dendritic compartment are shown in Fig. 2 (the corresponding line-scan profile is shown in Fig. 1 *A*). They had variations that were, at least for large τ, larger than the noise of the ACF. At first glance, dendritic ACFs could be fitted by a one-component model (Eq. 11 for $m = 1$, Fig. 3 *A*), but the fit was never satisfactory (Fig. 3 *C*). Using a two-component model (Eq. 11, $m = 2$) (Fig. 3 *B*) led to considerably smaller residues (Fig. 3 *D*), apparently indicating the existence of two molecular species.

In many cases, however, even a two-component model did not converge well and a third component had to be assumed. Figure 4 gives an example of such an ACF showing a characteristic shoulder for large τ. A stationary ACF shoulder of this shape is characteristic of stationary uniform translation processes (Magde et al., 1978), whereas a sudden onset and subsequent decay is caused by a single transient event (STE, see above). In fact, a satisfactory approximation was obtained using an ACF model with two terms for confined diffusion according to Eq. 11 (summation index $j = 1, 2$), and another one for an STE according to Eq. 21 (summation index $j = 3$) (Fig. 4).

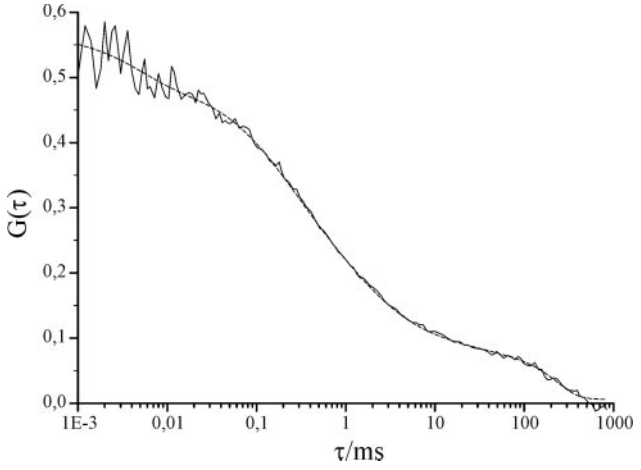

FIGURE 4 ACF with STE component, calculated from fluorescence fluctuations of 10 kDa TMR-dextran emitted from a dentrite of a cultured neuron of the OB (identical to the upper trace of Fig. 2). Fitting a three-component model with two components of normal, confined diffusion (Eq. 11, summation index $j = 1, 2$) and one component for an STE (Eq. 21, summation index $j = 3$) gave $\langle N_{tot} \rangle = 2.012$, $T = 0.134$, $\tau_T = 4.64$ μs, $\Phi_1 = 0.499$, $\tau_{diff_1} = 0.209$ ms, $\Phi_2 = 0.375$, $\tau_{diff_2} = 1.573$ ms, $\Phi_3 = 0.114$, and $\tau_{t_3} = 239.5$ ms (fixed parameter: $Y = 3.79$).

Evaluating dendritic FCS data consistently led to two or three components with relative contributions Φ_1, Φ_2, and Φ_3 and time constants τ_{diff_1}, τ_{diff_2} and τ_{t_3} or τ_{diff_3}, respectively. Plotting the time constants τ_{diff_1} (first component), τ_{diff_2} (second component), and τ_{t_3} or τ_{diff_3} (third component) for the six subsequent recordings of the experiment shown in Fig. 2 revealed that two of the time constants show a surprisingly small variance and average values of 189 μs and 1.626 ms, respectively (Fig. 5, *A* and *B*), whereas the third one fluctuated markedly. In this case, the third component could be described either by a third diffusional component (Φ_3, τ_{diff_3}) or by an STE (Φ_3, τ_{t_3}).

Plotting the relative contributions Φ_1, Φ_2, and Φ_3 as a function of the time constant τ showed that the narrowly distributed contributions Φ_1 and Φ_2 are on the order of magnitude of 55 and 40%, whereas the third component (τ_{diff_3} in case of diffusion, τ_{t_3} in case of an STE), which varied between 10 ms and more than 200 ms, contributed about 10% or less to the ACF (Fig. 5 *B*). Note that the third component was absent in some recordings (e.g., Fig. 5 *A*, recording index $i = 2$).

Taken together, analyzing dendritic diffusion using the model for confined diffusion leads to the confusing result that two or three molecular species have to be assumed though just one had been added to the cytosol. This apparent contradiction raises some questions, which we will answer in the following sections:

1. Is there anything particular about dendritic diffusion that cannot be observed in somata? This question led us to perform FCS measurements in somata and to compare them to results obtained in dendrites.

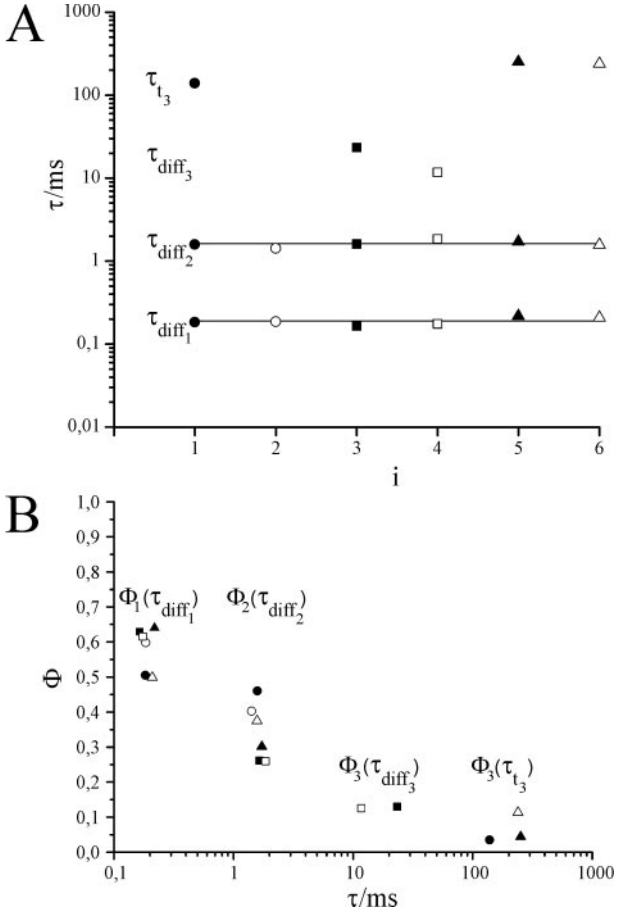

FIGURE 5 Parameter representation of the subsequent ACFs shown in Fig. 2. (*A*) Fitted diffusion and transition time constants of six individual recordings (recording index *i*). The two horizontal lines are the mean values $\bar{\tau}_{diff_1} = 0.189$ ms and $\bar{\tau}_{diff_2} = 1.626$ ms of the first and second diffusion time constants, respectively. (*B*) Relative contributions Φ_j of the fluorescent species to the ACFs as a function of fitted time constants.

2. Are there autofluorescent species in addition to the exogenous fluorophore that contribute to the ACF? To test this we did experiments in cells with no TMR-dextran added.
3. Does the dendritic cytoarchitecture, in particular the microtubulus network, introduce an anisotropy? If so, intradendritic diffusion must be described by a model that distinguishes diffusion along the dendrite from diffusion across the dendrite. We set up such a model (Eqs. 15–19) and applied it to data taken from dendrites.
4. Does TMR-dextran bind to cytosolic constituents or the plasma membrane? We investigated this possibility by measuring diffusion in thin dendrites, which can be modeled as standard one-dimensional (1D) diffusion.
5. Is our model for confined diffusion possibly flawed in a way that leads to apparent fluorescent species? We checked this by measuring ACFs in thick dendrites where the standard model for two-dimensional (2D) or 3D diffusion can be used. We then determined the number of components under these conditions.

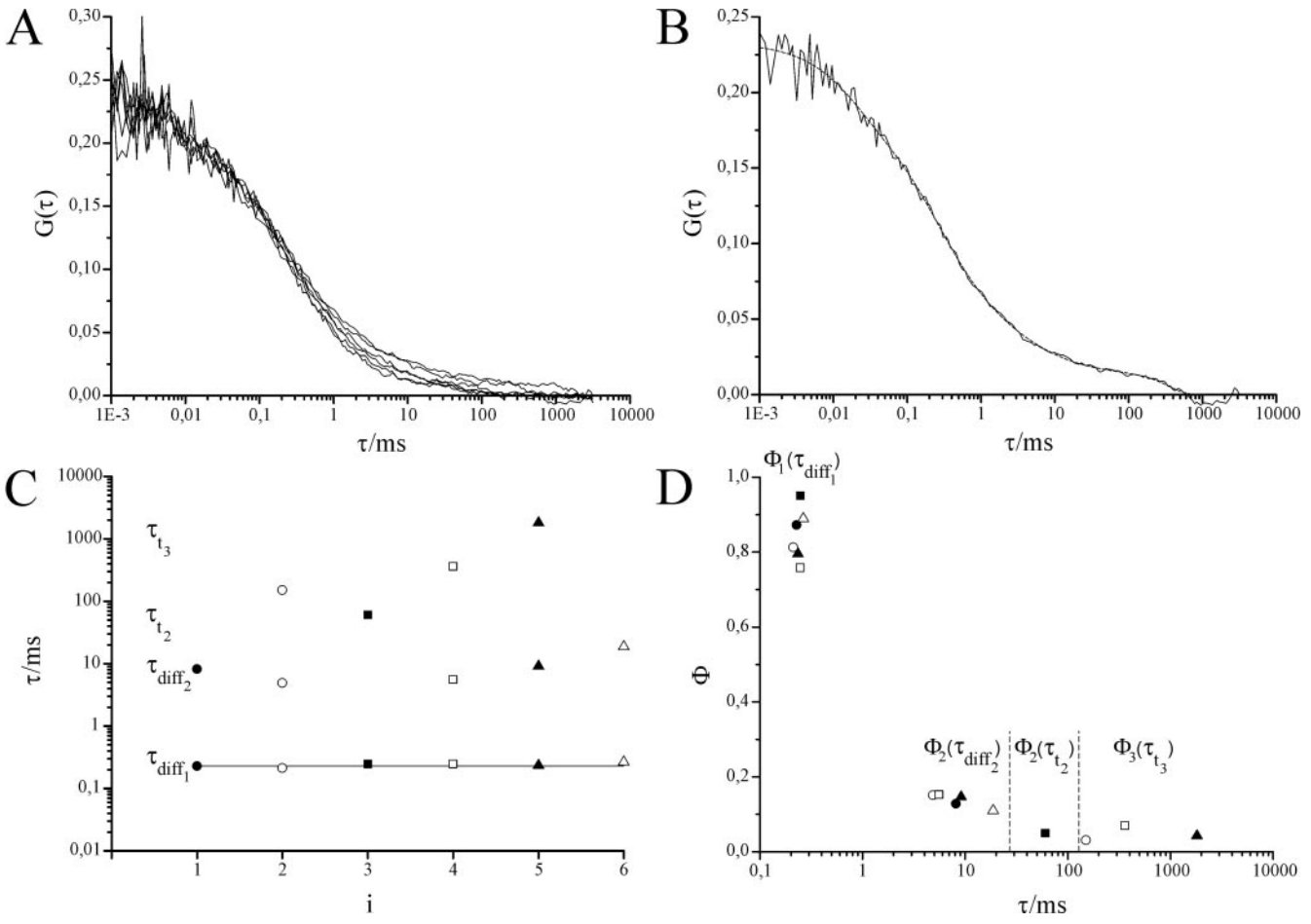

FIGURE 6 ACFs calculated from fluorescence fluctuations of 10 kDa TMR-dextran emitted from a soma of a cultured neuron of the OB. Each of the subsequent ACFs was measured over 10 s in the same somatic compartment (the time delay between two measurements was ~10 s). The measurements were carried out after diffusion had reached a steady state. (*A*) ACFs of six subsequent measurements. (*B*) ACF with STE component. Fitting an ACF model with two components according to Eq. 10 (summation index $j = 1, 2$) and one STE component (Eq. 21, summation index $j = 3$) gave $\langle N_{tot} \rangle = 5.14$, $T = 0.18$, $\tau_T = 1.73$ μs, $\Phi_1 = 0.76$, $\tau_{diff_1} = 0.246$ ms, $\Phi_2 = 0.153$, $\tau_{diff_2} = 5.57$ ms, $\Phi_3 = 0.07$, and $\tau_{t_3} = 360.62$ ms (fixed parameter: $S = 7$). (*C*) Fitted diffusion and transition time constants of the ACFs shown in *A* (recording index *i*). The horizontal line denotes the mean $\bar{\tau}_{diff_1} = 0.239$ ms of the first diffusion time constant τ_{diff_1}. (*D*) Relative contributions Φ_j of the fluorescent species as a function of the fitted time constants plotted in *C*. The dye concentration within the soma was ~15 nM.

Diffusion in somata differs from diffusion in dendrites

Somatic ACFs, like dendritic ACFs, showed marked fluctuations (Figs. 6 *A* and 7 *A*), which partly appeared to be based upon STEs of large molecules (Fig. 6 *B*). Because the somatic width and height (d_y, $d_z \geq 6$ μm) are sufficiently larger than the width and hight of the detection volume (with $r_{xy} \cong 0.24$ μm and $S \cong 7$, we find $Y = d_y/r_{xy} \geq 25$ and $Z = d_z/r_z \geq 3.53$, see Gennerich and Schild, 2000), the confinement of diffusion due to the somatic plasma membrane can be neglected. We therefore fitted the somatic ACFs using the standard diffusion model (Eq. 10). In contrast to our findings in dendrites, only one fluorescent component of the soma was constant over subsequent recordings (Figs. 6 *C* and 7 *C*). This component contributed 75–95% (Fig. 6 *D*) and 90–100% (Fig. 7 *D*) to the total ACF, respectively, whereas the fluctuating second and third diffusion time constants contributed little to the total ACF (Figs. 6 *D* and 7 *D*). Similar results were observed in 67 somata. In many cases, a one-component FCS model (Eq. 10, $m = 1$) with $\Phi_1 = 1$ (Fig. 7 *D*) was therefore sufficient to obtain a satisfactory fit (Fig. 7, *B* and *C*, recording index $i = 1, 3$).

The predominant first time constant τ_{diff_1} was found to be 1.2–2.6 times larger with respect to aqueous solution ($\tau_{diff} = 0.16$ ms for our set-up), indicating a relatively free and rapid diffusion of a macromolecule-sized solute in somata. The fluctuating components observed in both somata and dendrites may be brought about by large autofluorescent particles (e.g., autofluorescent mitochondria, *arrow* in Fig. 9 *A*; see also, Brock et al., 1998) diffusing or being transported through the focal volume. Note, however, that the second stationary component τ_{diff_2} as measured in dendrites was never observed in somata. It therefore appears to be specific for dendritic diffusion.

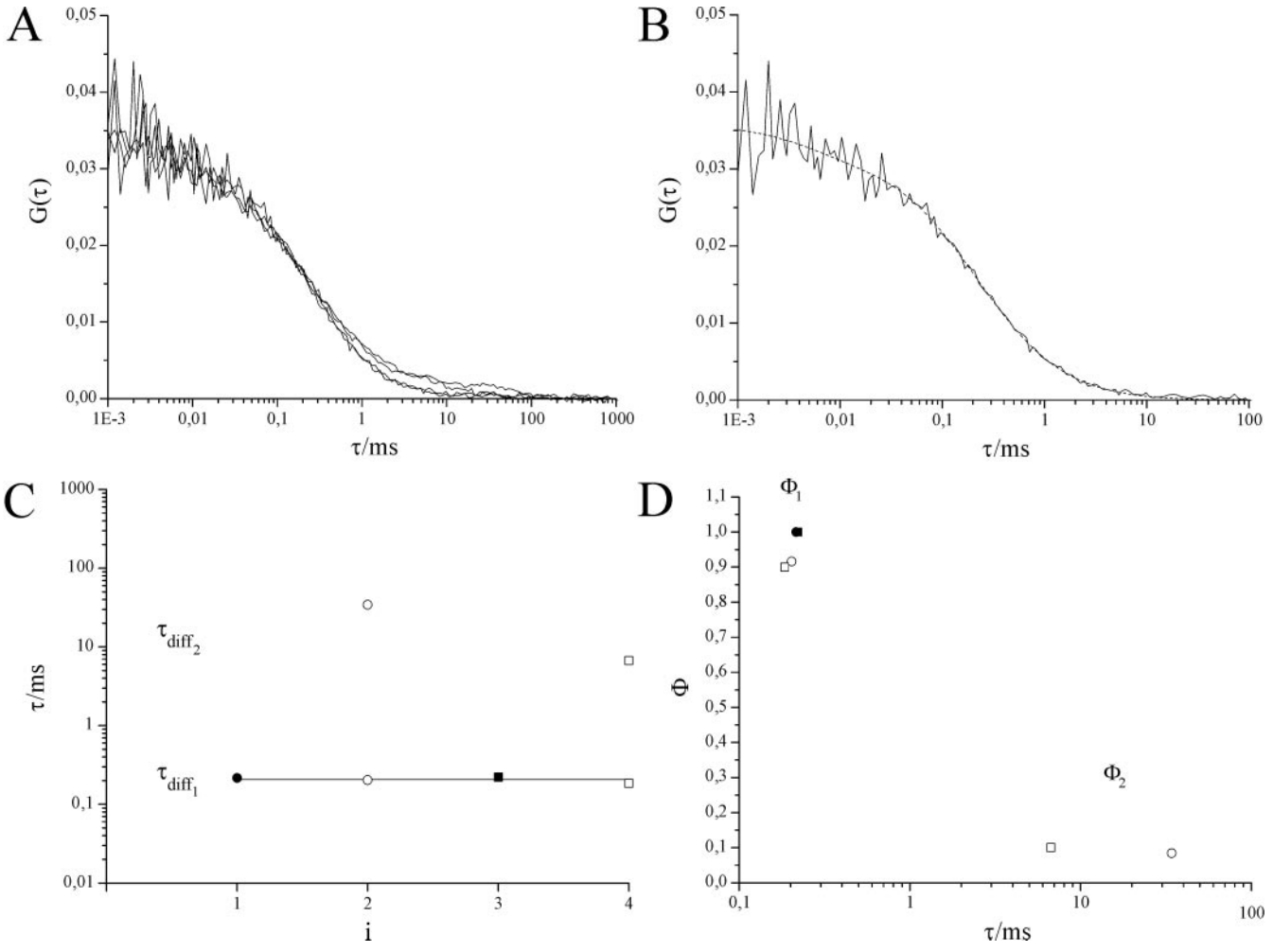

FIGURE 7 ACFs calculated from fluorescence fluctuations of 10 kDa TMR-dextran emitted from a soma of a cultured neuron of the OB. The ACFs were measured over 2.6–7.7 s in the same somatic compartment (the time delay between two measurements was ~10 s). The measurements were carried out after diffusion had reached a steady state. (*A*) ACFs of four subsequent measurements. (*B*) ACF identical to one of the lower curves shown in *A* (measurement time: $t_m = 2.6$ s). Fitting an ACF model with one component according to Eq. 10 gave: $\langle N \rangle = 31.21$, $T = 0.109$, and $\tau_{diff_1} = 0.216$ ms (fixed parameter: $\tau_T = 4$ μs and $S = 7$). (*C*) Fitted diffusion time constants of the ACFs shown in *A* (recording index *i*). The horizontal line denotes the mean value $\bar{\tau}_{diff_1} = 0.206$ ms of the first diffusion time constant τ_{diff_1}. (*D*) Relative contributions Φ_j of the fluorescent species as a function of the fitted time constants plotted in *C*. The dye concentration within the soma was calculated to be ~100 nM ($\langle C \rangle = \langle N \rangle / V_d N_A$, $V_d = 0.51$ fl).

Transient autofluorescent particles

Many recordings showed infrequent fluorescence peaks that led to additional transient ACF contributions that were best fitted by Eq. 21. The fits resulted in large transition times τ_t (e.g., $\tau_{t_3} = 360.62$ ms for the ACF shown in Fig. 6 *B*, and below $\tau_t = 292$ ms and $\tau_t = 222$ ms for the two upper curves shown in Fig. 11 *A*). We tentatively interpreted these events as large autofluorescent intracellular particles passing through the focus volume at random times. This hypothesis was confirmed by recordings from dendrites of cultured neurons that had not been filled with TMR-dextran. Figure 8 shows ACFs recorded under such conditions. The lower ACF, which corresponds to the fluorescence count rate in the left inset (0–7 s) contains just a noise component brought about by uncorrelated back-scattering light of the exciting laser beam. However, the fluorescence emission peaked at random times (Fig. 8, *right inset*, 18–26 s), and whenever this happened the ACF made a "jump" to assume transiently a shape as shown in the upper trace of Fig. 8. Such ACFs could be approximated by the FCS model for STEs (Eq. 21) with time constants in the range of 5–1200 ms, i.e., identical to the STEs observed in dendrites filled with TMR-dextran.

Anisotropic dendritic diffusion

In mitral-cell dendrites, there is a regular network of microtubuli (Fig. 9) along the dendrite, suggesting approximately free diffusion in the direction along the dendrite but hampered diffusion across the dendrite. We therefore as-

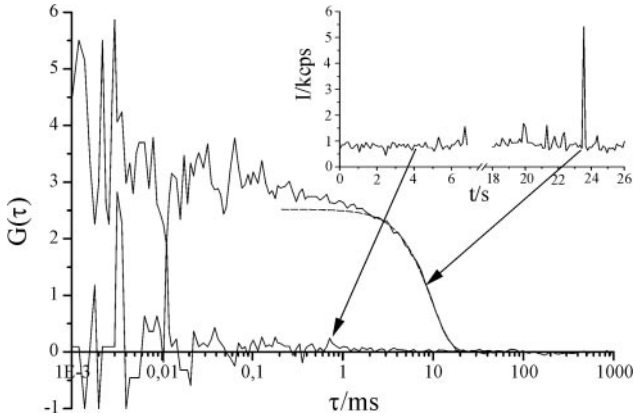

FIGURE 8 Autocorrelation curves calculated from autofluorescence fluctuations emitted from a dentrite of a cultured OB neuron that was not filled with TMR-dextran. The lower curve shows the ACF calculated from the fluctuations shown in the left inset (0–7 s, background intensity $I_B \approx$ 0.8 kcps), and the upper curve shows the ACF obtained from the fluorescence fluctuations shown in the right inset (18–26 s). Fitting the upper curve with an STE component (Eq. 21) gave $\tau_t = 9.57$ ms (*dashed curve*).

sumed that dendritic diffusion was anisotropic and approximated dendritic FCS data using a model for anisotropic diffusion (Eq. 17). Fitting this model to dendritic ACFs without STE contribution (e.g., Fig. 2, *lowest curve*; see also Fig. 5 *A*, recording index $i = 2$) indeed suggest one component with $\Phi_1 = 1$ (Fig. 10). The data shown in Fig. 2 lead to characteristic time constants $\tau_{\text{diff}_\parallel}$ and $\tau_{\text{diff}_\perp}$ for diffusion parallel and orthogonal to the dendrite, $\tau_{\text{diff}_\parallel} = (0.179 \pm 0.011)$ ms and $\tau_{\text{diff}_\perp} = (14.62 \pm 2.75)$ ms. In this example, the mobility of 10 kDa TMR-dextran, as compared to its mobility in water ($\tau_{\text{diff}} = 0.16$ms), was thus reduced by a factor of 1.1 along the dendrite and by a factor of 91 across the dendrite. Diffusion is thus markedly slower in directions orthogonal to the dendritic axis. Similar results were measured in 61 dendrites. Table 1 gives a summary of the measured dendritic and somatic diffusion constants. D_{aq} of 10 kDa TMR-dextran (100 nM) measured in a drop of water gave the value $D_{\text{aq}} = (8.5 \pm 0.3) \times 10^{-7}/\text{cm}^2/\text{s}$.

We tried to support our interpretation of anisotropic diffusion by the following experiment: We incubated the cultured cells adding nocodazole or colchicine (10 μg/ml each, Sigma-Aldrich Chemie) to the culture medium to disrupt the microtubules. Both drugs inhibit polymerization of tubulin. After two days of incubation, the microtubules started to disaggregate as evidenced by antibody staining against α-tubulin (not shown). At the same time, the dendritic cross sections became irregular and FCS measurements led to inconsitent results. Occasionally, the geometry of a dendritic compartment could still be approximated by a circular or rectangular shape. In those cases, there was just one characteristic diffusion time constant, which was in the same range as the predominant time constant found in somata (not shown).

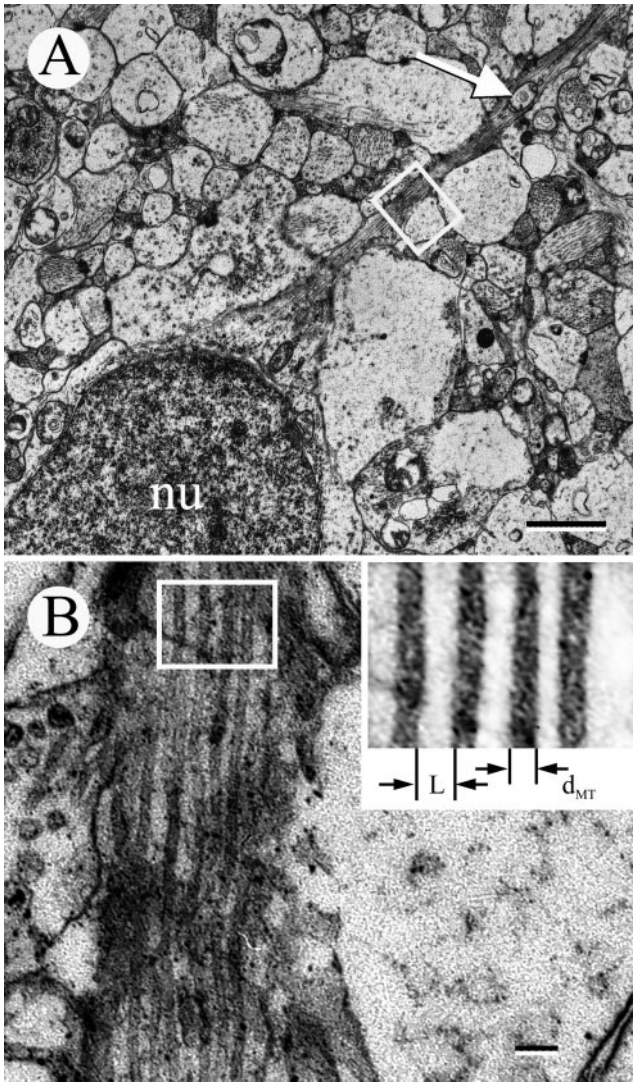

FIGURE 9 Transmission electron micrographs of a mitral cell dendrite. (*A*) Low magnification of the soma (*lower left*) and a dendrite with mitochondrium (*arrow*). The nucleus (*nu*) occupies most of the volume of the soma. Scale bar: 2 μm. (*B*) Higher magnification of the region indicated in *A*. Note the parallel arrangement of microtubuli along the dendrite. Scale bar: 100 nm. The inset shows a higher magnification with digitally increased contrast of the region indicated in *B*. *L* denotes the distance between adjacent microtubuli and d_{MT} the microtubular diameter.

Binding of TMR-dextran to cellular elements

Though the above interpretation of anisotropic dendritic diffusion may appear plausible, two potential artifacts seem possible. First TMR-dextran may bind to or interact with cytosolic elements or the plasma membrane, and second, our model for confined diffusion itself might introduce an apparent time constant. We therefore carried out experiments in dendrites with diameters of 200 nm or less. In such dendrites, diffusion in the lateral direction (y–z plane) can be neglected because, with $r_{xy} = 0.24$ μm and $r_z = 1.7$ μm, we have $Y = d_y/r_{xy} \leq 0.83$ and $Z = d_z/r_z < 0.83$, i.e., the

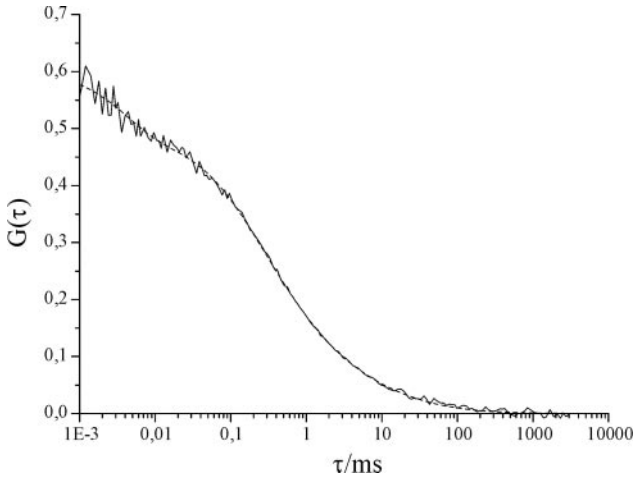

FIGURE 10 Autocorrelation function calculated from fluorescence fluctuations of 10 kDa TMR-dextran emitted from a dentrite of a cultured neuron of the OB (identical to the lowest trace shown in Fig. 2). Fitting the model of anisotropic confined diffusion (Eqs. 17, 18, and 19, *dashed curve*) gave $\langle N \rangle = 2.074$, $T = 0.207$, $\tau_T = 4.23\ \mu s$, $\tau_{diff_\parallel} = 0.172$ ms, and $\tau_{diff_\perp} = 15.85$ ms (fixed parameter: $Y = d_y/r_{xy} = 3.79$, taken from the line-scanning measurement of this dendrite, Fig. 1 *A*).

dendritic width and height are sufficiently smaller than the width and height of the detection volume (Gennerich and Schild, 2000). In these cases, the 1D model for diffusion along the dendritic axis must be applied (Eq. 16). Figure 11 *A* shows an example of subsequent FCS measurements taken from a dendrite with a diameter of ~190 nm (line-scan profile, Fig. 11 *D*). Here we could easily distinguish between stationary ACFs and ACFs reflecting STEs (*two upper curves* in Fig. 11 *A*). The stationary ACFs (*lower curves* in Fig. 11 *A*) could be well fitted with a one-component model (1D-ACF $G_x(\tau)$, Eq. 16) (Fig. 11 *B*), suggesting only one fluorescent species. For the two upper curves, we obtained a satisfactory approximation by using an ACF model with one term for 1D diffusion and a second one for an STE (Eq. 21; $\tau_t = 292$ ms for the upper curve and $\tau_t = 220$ ms for the second curve from the top, see Fig. 11 *C*). For the stationary curves, the characteristic diffusion time constant gave a value of $\tau_{diff_\parallel} = (0.233 \pm 0.013)$ ms, which is in the range of the first stationary diffusion time constant τ_{diff_1} found in thicker dendrites and analyzed with a 2D diffusion model.

A second stationary diffusion time constant τ_{diff_2}, as it would arise from TMR-dextran bound to some other molecule, was never observed in these experiments. Binding to cytosolic elements or the plasma membrane can thus be ruled out. The second diffusion time constant τ_{diff_2} could therefore be attributed to dendritic 2D diffusion as discussed above.

Diffusion in thick dendrites

As a last source of apparent fluorescent species, we considered a potential flaw of our model for confined diffusion (Eq. 11). The data shown so far were all taken from dendrites the line-scan profiles of which were best decribed by rectangular cross-sections (see Fig. 1 *A*). "Best described" does, of course, not mean perfectly described, and thus the boundary conditions of the diffusion model are not perfectly correct. This might be responsible for the appearance of an additional time constant, which should thus be absent in thick dendrites, where the standard diffusion model can be applied (for critical values, see Gennerich and Schild, 2000).

We carried out FCS measurements in thick dendrites. Figure 12 *A* shows ACFs of a dendrite the radius of which was 1.64 μm (Fig. 1 *B* gives the line-scan profile of this dendrite). Characteristic diffusion times were assessed using the standard 3D diffusion model (Eq. 10) or its analog for (unconfined) anisotropic diffusion (Eq. 15). Figure 12 *B* shows the characteristic time constants obtained from part *A* of the figure and it is obvious that two of them are essentially unchanged over time. The third time constant (*upper traces* in Fig. 12 *A*) presumably reflect STEs. The STE-free traces in Fig. 12 *A* could all be fitted using the standard model for two fluorescent species (Fig. 12 *C*). Fitting the one-component model was not satisfactory (Fig. 12 *C*). Therefore, the appearance of two time constants is not brought about by the model of confined diffusion. The above interpretation of anisotropic diffusion is thus the most plausible explanation of our data. In fact, the STE-free traces obtained in thick dendrites (*lower traces* in Fig. 12 *A*) could be fitted using the model of unconfined anisotropic diffusion (Eq. 15) of one fluorescent species (Fig. 12 *D*).

TABLE 1 Mobilities of 10 kDa TMR-dextran in cultured OB neurons

Cytosolic compartment	Soma/Nucleus (Number of cells)	Dendrite* (Number of dendrites)
$[D] = 10^{-7}$ cm^2/s	$3.4 \le D_{cyto} \le 7.3$ (67)	$4.1 \le D_{cyto_\parallel} \le 7.9$ (88)
	$1.2 \le D_{aq}/D_{cyto} \le 2.6$	$1.1 \le D_{aq}/D_{cyto_\parallel} \le 2.1$
		$0.085 < D_{cyto_\perp} < 0.89$ (73)
		$9.6 < D_{aq}/D_{cyto_\perp} < 100$

*The dendritic diffusion data contain results from thick and thin dendrites (see below) and from intermediate-sized dendrites.

DISCUSSION

The diffusion constant D_{cyto} of TMR-dextran (10 kDa) in the center of mitral-cell somata, i.e., in the nucleus, was 1.2–2.6 times smaller than in water, indicating relatively unhampered diffusion in the nucleus. Similar results have been reported by Politz et al. (1998) for the diffusion of fluorescein-labeled oligodeoxynucleotides (with similar diffusion constants to that one of 10 kDa TMR-dextran) inside the nucleus of cultured rat myoblasts. For a large fraction of intranuclear oligo(dT) and oligo(dA) they found a 1.2 and 1.4 times reduced mobility with respect to water, respec-

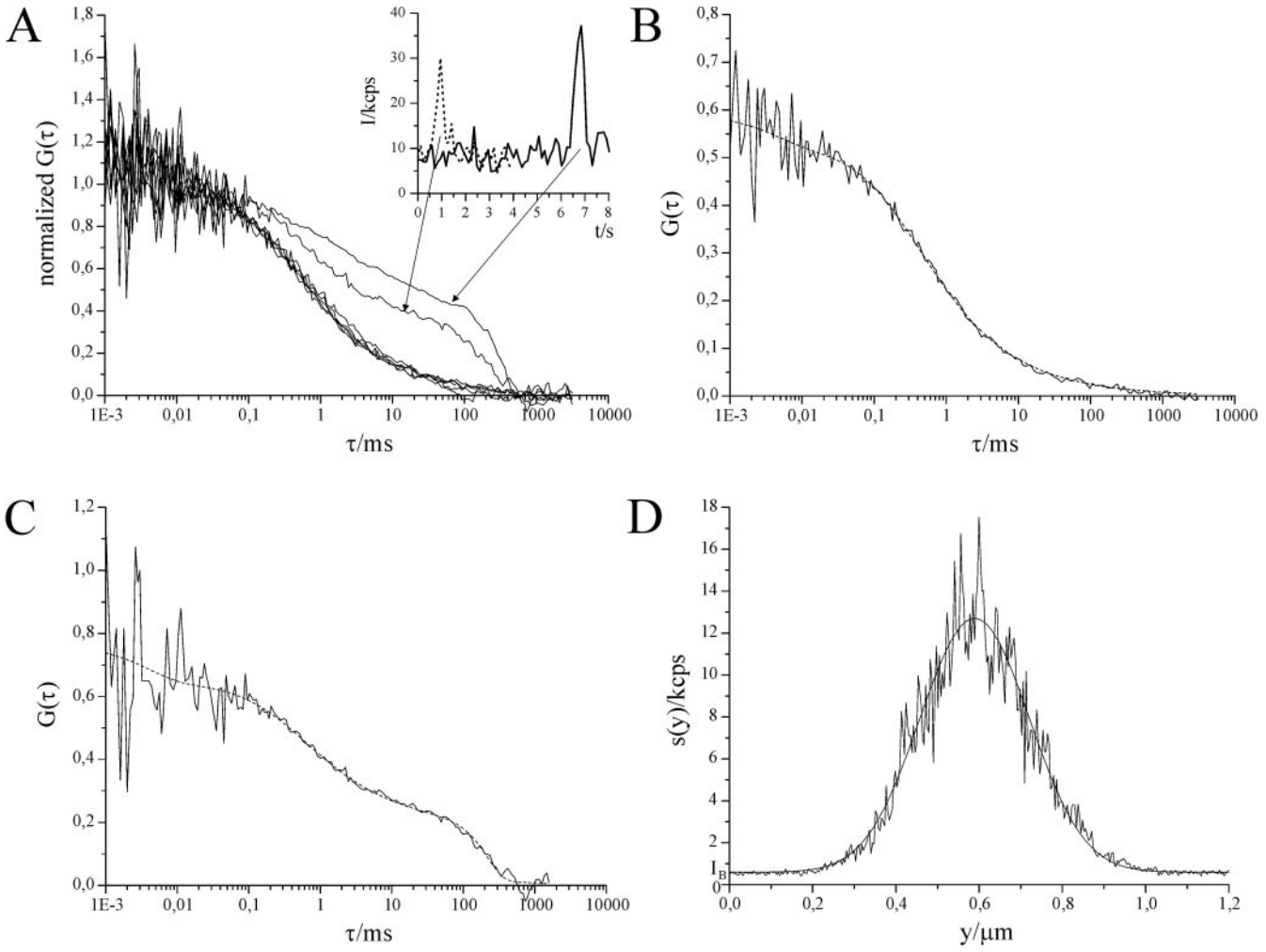

FIGURE 11 FCS and line-scan measurements carried out on a thin dendrite of a cultured neuron of the OB that was filled with 10 kDa TMR-dextran. (*A*) ACFs, normalized by the average number of molecules $\langle N \rangle$, of the subsequent measurements. The duration of each FCS measurement was between 4 and 8 s. The two upper curves correspond to the fluorescence fluctuations shown in the inset (upper ACF: *solid intensity trace*; second ACF from the top: *dashed intensity trace*; background intensity $I_B = 0.6$ kcps). The time delay between two measurements was ~10 s. (*B*) One of the lower stationary ACFs shown in *A* (non-normalized). Fitting the one-component 1D model $G_x(\tau)$ (Eq. 16) gave $\langle N \rangle = 1.893$, $T = 0.107$, $\tau_T = 4.27$ μs, and $\tau_{diff_\parallel} = 0.217$ ms. (*C*) ACF containing an STE component (identical to the second curve from top shown in *A*). Fitting a two-component model with one component for normal 1D diffusion (Eq. 16) and one component for an STE (Eq. 21) gave $\langle N_{tot} \rangle = 1.548$, $T = 0.156$, $\Phi_1 = 0.707$, $\tau_{diff_\parallel} = 0.318$ ms, and $\tau_t = 221.74$ ms (fixed parameter: $\tau_T = 4$ μs). (*D*) Line-scan through a thin dendrite of a cultured neuron that was homogeneously filled with TMR-dextran (10 kDa) (*noisy trace*) (the corresponding FCS measurements are shown in *A*); scan velocity: 38 nm/s. The theoretical line-scan profile $s'_{rect}(y)$ (Eq. 8) for a rectangular dendritic cross section was fitted (*solid curve*) to the experimental line-scan profile. Result of the fit: $\beta = 10.45$ kcps, $d_y = 0.19$ μm, $y_0 = 0.589$ μm, and $I_B = 0.599$ kcps, respectively (fixed parameter: $r_{xy} = 0.236$ μm).

tively. However, several investigators found lower mobilities, e.g., a 3–5 times reduced mobility for a green fluorescent protein mutant (EGFP, about the same diffusion constant as 10 kDa TMR-dextran) in AT-1, COS-7 (Wachsmuth et al., 2000), and RBL cells (Schwille et al., 1999), as well as a 4 times slower diffusion for 10 kDa Cy3-labeled dextran in A431 and Her-14 cell lines (Brock et al., 1998).

FCS measurements in dendrites pose a problem, because the diameter of the dendrites is typically on the same order of magnitude or smaller than that of the FCS detection volume. The diffusion volume is thus confined by the plasma membrane. We therefore applied an FCS model for confined diffusion (Gennerich and Schild, 2000).

Our FCS measurements in dendrites, performed with TMR-dextran (10 kDa) added through a patch pipette, led to the puzzling finding that more than one fluorescent species was detected though only one species was added to the cytosol. This finding needed an explanation.

We considered some physiological, artifactual, and methodological sources that could possibly give rise to a second or third time constant. First, we could rule out that 10 kDa TMR-dextran binds to intracellular components (Fig. 11).

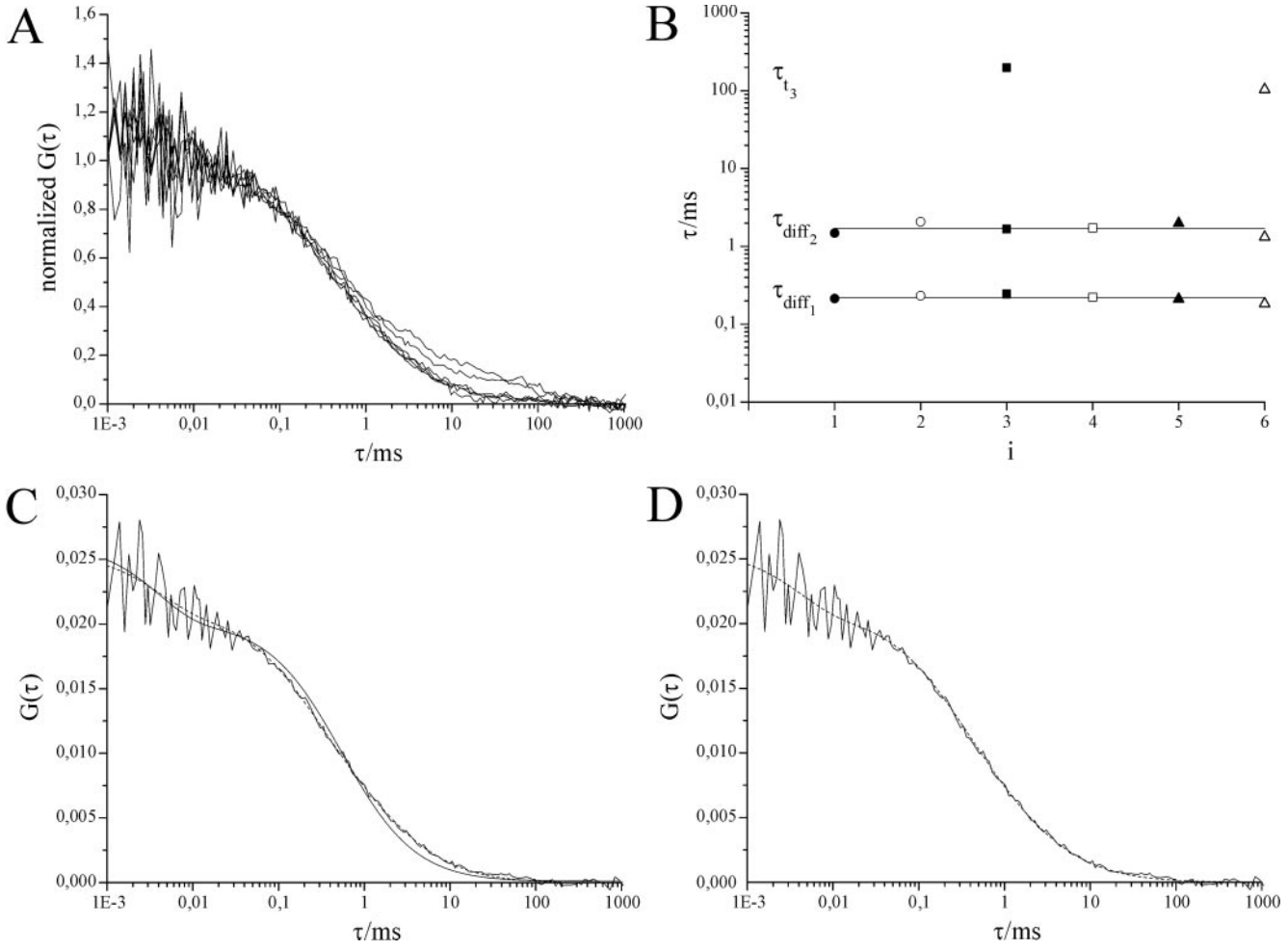

FIGURE 12 Autocorrelation plots and parameter representation from FCS measurements carried out on a thick dendrite of a cultured neuron of the OB. (*A*) ACFs, normalized by the average number of molecules $\langle N_{tot}\rangle$, calculated from fluorescence fluctuations of 10 kDa TMR-dextran emitted from the center of the dendrite (Fig. 1 *B* shows the line-scan profile of this dendrite). The duration of each FCS measurement was ~5 s to reduce the detection probability of STEs. The time delay between two measurements was ~10 s. (*B*) Fitted diffusion and transition time constants plotted over the recording index *i*. The two horizontal lines are the mean values $\bar{\tau}_{diff_1} = 0.217$ ms and $\bar{\tau}_{diff_2} = 1.71$ ms of the first and second diffusion time constants with the contributions Φ_1 and Φ_2 of 60 and 40%, respectively. Due to the confinement of diffusion along the *z* axis ($Z = d_z/r_z = 2R/r_z = 1.981$, with $r_z = 1.652$ μm) together with the large structure factor of $S = 7$, virtually identical time constants resulted from the standard two-component 2D-ACF model (not shown). Because the dendritic width was sufficiently larger than the width of the detection volume (with $d_y = 2R = 3.27$ μm and $r_{xy} = 0.236$ μm, we find $Y = d_y/r_{xy} = 13.86$), the confinement of diffusion along the *y* axis was neglected. (*C*) ACF (*noisy trace*), identical to one of the lower stationary traces shown in *A*. Fitting the standard two-component model (Eq. 10, $m = 2$, *dashed curve*) gave $\langle N_{tot}\rangle = 47.38$, $T = 0.175$, $\Phi_1 = 0.621$, $\tau_{diff_1} = 0.211$ ms, and $\tau_{diff_2} = 1.99$ ms (fixed parameters: $\tau_T = 4$ μs and $S = 7$). Fitting the standard one-component model (Eq. 10, $m = 1$, *solid curve*) gave $\langle N\rangle = 49.64$, $T = 0.233$, and $\tau_{diff_1} = 0.561$ ms (fixed parameters: $\tau_T = 4$ μs and $S = 7$). (*D*) Fitting the model for anisotropic nonconfined diffusion (Eq. 15, *dashed curve*) to the ACF shown in *C* gave $\langle N\rangle = 47.98$, $T = 0.191$, $\tau_{diff_\parallel} = 0.187$ ms, and $\tau_{diff_\perp} = 4.169$ ms (fixed parameters: $\tau_T = 4$ μs and $S = 7$). The dendritic dye concentration was calculated to be ~170 nM ($\langle C\rangle = \langle N_{tot}\rangle/V_d^* N_A$, with $V_d^* = \pi^{3/2} r_{xy} r_z [\mathrm{erf}(Z/\sqrt{2})]^2/\mathrm{erf}(Z) = 0.467$ fl, see Gennerich and Schild, 2000).

Second, we ruled out that our model for confined diffusion might have generated artifactual time constants (Fig. 12). In contrast, we could show that the second stationary diffusion time constant did not occur in somata (Fig. 6 and 7). It appeared, in fact, to be characteristic for dendrites.

As shown in Fig. 9, the most obvious difference between the somatic and dendritic cytosceleton is the regular network of parallel microtubuli found in dendrites. This, together with the fact that the contributions Φ_1 and Φ_2 for the first and second diffusion time constant, τ_{diff_1} and τ_{diff_2}, were approximately equal, suggested that the two (approximately) equal components might physically correspond to one molecular species that diffuses differently in different directions.

The distance *L* between adjacent microtubuli of mitral cell dendrites (see inset of Fig. 9 *B*) was in the range 10–80 nm, whereas the average microtubular diameter d_{MT} was determined to be ~20 nm. The average hydrodynamic diameter d_h of the 10 kDa TMR-dextran follows from the Stokes–Einstein equation, i.e., $d_h = kT/3\pi\eta D_{aq} = 5.1$ nm

(D_{aq}, dextran diffusion constant). From these values, it appeared plausible that the microtubular network hampered diffusion across the dendrite (on the length scale of r_{xy}) while leaving it largely unaffected along the dendrite.

The stationary dendritic FCS data could indeed be fitted with a one-component model for anisotropic diffusion. The results suggested a 1.1–2.1 reduced mobility for diffusion along the dendrite, whereas the diffusion of the 10 kDa TMR-dextran in lateral direction was 10–100 times slower.

The assumption of anisotropic diffusion leads to a physically plausible view of diffusion in dendrites. With one fluorescent species added to a cell through a patch pipette, one fluorescent species is detected, plus autofluorescence when present.

We thank Dr. Leonid Nezlin (University of Göttingen, Dept. of Molecular Neurophysiologie, Germany) for kindly providing the electron micrographs and our technical assistants Mrs. Gudrun Federkeil and Mr. Joško Kuduz, for the preparation of the cell culture.

REFERENCES

Aragón, S. R., and R. Pecora. 1976. Fluorescence correlation spectroscopy as a probe of molecular dynamics. *J. Chem. Phys.* 64:1791–1803.

Bischofberger, J., H. Geiling, J. Engel, H. A. Schultens, and D. Schild. 1995. A cultured network of olfactory bulb neurons of *Xenopus laevis* tadpoles: calcium imaging and spontaneous activity. *In* Advances in the Biosciences. Vol. 93. Chemical Signals in Vertebrates, R. Apfelbach, D. Müller-Schwarze, K. Reutter, and E. Weiler, editors. Elsevier, Oxford, U.K. 133–139.

Bischofberger, J., and D. Schild. 1995. Different spatial patterns of Ca^{2+} increase by N- and L-type Ca^{2+} channel activation in frog olfactory bulb neurones. *J. Physiol.* 487:305–317.

Brock, R., M. A. Hink, and T. M. Jovin. 1998. Fluorescence correlation microscopy of cells in the presence of autofluorescence. *Biophys. J.* 75:2547–2557.

Czesnik, D., L. Nezlin, J. Rabba, B. Müller, and D. Schild. 2001. Noradrenergic modulation of calcium currents and synaptic transmission in the olfactory bulb of *Xenopus laevis* tadpoles. *Eur. J. Neurosci.* 13: 1093–1100.

Elson, E. L., and D. Magde. 1974. Fluorescence correlation spectroscopy. I. Conceptual basis and theory. *Biopolymers.* 13:1–27.

Gennerich, A., and D. Schild. 2000. Fluorescence correlation spectroscopy in small cytosolic compartments depends critically on the diffusion model used. *Biophys. J.* 79:3294–3306.

Magde, D., W. W. Webb, and E. L. Elson. 1978. Fluorescence correlation spectroscopy. III. Uniform translation and laminar flow. *Biopolymers.* 17:361–376.

Nieuwkoop, P. D., and J. Faber. 1956. Normal Table of *Xenopus laevis* (Daudin). North Holland Co., Amsterdam, The Netherlands.

Politz, J. C., E. S. Browne, D. E. Wolf, and T. Pederson. 1998. Intranuclear diffusion and hybridization state of oligonucleotides measured by fluorescence correlation spectroscopy in living cells. *Proc. Natl. Acad. Sci. U.S.A.* 95:6043–6048.

Rigler, R., Ü. Mets, J. Widengren, and P. Kask. 1993. Fluorescence correlation spectroscopy with high count rate and low background: analysis of translational diffusion. *Eur. Biophys. J.* 22:169–175.

Schwille, P., J. Bieschke, and F. Oehlenschläger. 1997. Kinetic investigations by fluorescence correlation spectroscopy: the analytical and diagnostic potential of diffusion studies. *Biophys. Chem.* 66:211–228.

Schwille, P., U. Haupts, S. Maiti, and W. W. Webb. 1999. Molecular dynamics in living cells observed by fluorescence correlation spectroscopy with one- and two-photon excitation. *Biophys. J.* 77:2251–2265.

Schwille, P. 2001. Fluorescence correlation spectroscopy and its potential for intracellular applications. *Cell. Biochem. Biophys.* 34:383–408.

Trombley, P. Q., and G. L. Westbrook. 1990. Excitatory synaptic transmission in cultures of rat olfactory bulb. *J. Neurophysiol.* 64:598–606.

Wachsmuth, M., W. Waldeck, and J. Langowski. 2000. Anomalous diffusion of fluorescent probes inside living cell nuclei investigated by spatially resolved fluorescence correlation spectroscopy. *J. Mol. Biol.* 298:677–689.

Widengren, J., Ü. Mets, and R. Rigler. 1995. Fluorescence correlation spectroscopy of triplet states in solution: a theoretical and experimental study. *J. Phys. Chem.* 99:13368–13379.

Widengren, J., and R. Rigler. 1998. Fluorescence correlation spectroscopy as a tool to investigate chemical reactions in solutions and on cell surfaces. *Cell. Mol. Biol.* 44:857–879.